

Ascorbate-Assisted Growth of Hierarchical ZnO Nanostructures: Sphere, Spindle, and Flower and Their Catalytic Properties

Manoj Raula, Md. Harunar Rashid, Tapas K. Paira, Enakshi Dinda, and Tarun K. Mandal*

Polymer Science Unit, Indian Association for the Cultivation of Science, Jadavpur, Kolkata 700 032, India

Received November 30, 2009. Revised Manuscript Received February 18, 2010

A simple solution-based method to prepare mainly flowerlike zinc oxide (ZnO) nanostructures using the ascorbate ion as a shape-directing/capping agent at relatively low temperature (ca. 30 and 60 °C) was described. However, we observed that different shapes of hierarchical ZnO nanostructures such as flowerlike, spindlelike, and spherical could be obtained with an increase in the synthesis temperature from 60 to 90 °C. The effects of other organic capping agents on the shape of hierarchical ZnO nanostructures were also studied. FTIR, FESEM, and XRD characterization were performed on the formed ZnO nanostructures to understand the role of ascorbate in the growth of flowerlike morphology. The nucleation and growth process can regulate by changing the metal precursor and ascorbate ion concentrations. We were able to identify intermediate nanostructures such as spherical/quasi-spherical and spindle that are very much on the pathway of formation of large, flowerlike ZnO nanostructures. Electron microscopy results indicated that these spherical/quasi-spherical ZnO nanoparticles might aggregate through oriented attachment to produce spindlelike and flowerlike nanostructures. On the basis of these results, a possible growth mechanism for the formation of flowerlike ZnO nanostructures was described. The optical properties of these differently shaped ZnO nanostructures were also described. The catalytic activities of the as-synthesized spherical and flowerlike ZnO nanostructures were tested in the Friedel–Crafts acylation reaction of anthracene with benzoyl chloride. The catalysis results indicated that the catalytic activity of flowerlike ZnO nanostructures is slightly higher than the spherical counterpart.

Introduction

Nanostructured zinc oxide (ZnO) is a versatile and technologically interesting semiconductor materials to study because it possesses very attractive physical properties such as a wide, direct band gap (3.37 eV),¹ a large exciton binding energy of 60 meV at room temperature, and unique acoustic,² catalytic,³ and electronic⁴ properties. Because of such versatile properties, it has great potential in applications such as room-temperature UV lasers,⁵ light-emitting diodes (LED),⁶ field-effect transistors,⁷ solar cells,⁸ sensors, and optoelectronics.⁹ These various applications require control of the morphology and dimensionality of the ZnO nanostructures. Consequently, several different synthesis approaches also come into effect to tune the size, shape, and hence the properties of such materials.

Among the various synthesis approaches, the vapor-phase growth of ZnO nanostructures is one of the most widely explored methods, which include chemical vapor deposition,¹⁰

thermal decomposition,¹¹ and thermal evaporation processes.¹² Although these techniques are suitable for obtaining high-quality crystalline ZnO nanostructures, they require sophisticated and expensive instrumental systems and/or toxic source materials and therefore may not be environmentally viable. Compared to the vapor-phase methods, solution-phase methods are very attractive and popular because they can be performed with good productivity without using any rigorous conditions or sophisticated instrumentation. Examples of such solution-phase methods include solvothermal,^{13–15} sol–gel,¹⁶ template-based,^{17–19} and templateless^{20–22} chemical methods. The chemistry involved in these techniques is the hydrolysis of zinc precursors under alkaline condition to form ZnO. There have been many reports on the preparation of ZnO nanostructures with a variety of new morphologies.^{3,13,17,19,20,23–30} The growth of these differently

*Corresponding author. Fax: 91-33-2473 2805. E-mail: psutkm@mahendra.iasc.res.in.

- (1) Monticone, S.; Tufeu, R.; Kanaev, A. V. *J. Phys. Chem. B* **1998**, *102*, 2854–2862.
- (2) Inoue, Y.; Okamoto, M.; Kawahara, T.; Morimoto, J. *J. Alloys Compd.* **2006**, *408–412*, 1234–1237.
- (3) Zhao, F.; Li, X.; Zheng, J.; Yang, X.; Zhao, F.; Wong, K. S.; Wang, J.; Lin, W.; Wu, M.; Su, Q. *Chem. Mater.* **2008**, *20*, 1197–1199.
- (4) Calhoum, M. F.; Sanchez, J.; Olaya, D.; Gershenson, M. E.; Podzorov, V. *Nat. Mater.* **2008**, *7*, 84–89.
- (5) Huang, M. H.; Mao, S.; Feick, H.; Yan, H.; Wu, Y.; Kind, H.; Weber, E.; Russo, R.; Yang, P. *Science* **2001**, *292*, 1897–1899.
- (6) Konenkamp, R.; Word, R. C.; Godinez, M. *Nano Lett.* **2005**, *5*, 2005–2008.
- (7) Ng, H. T.; Han, J.; Yamada, T.; Nguyen, P.; Chen, Y. P.; Meyyappan, M. *Nano Lett.* **2004**, *4*, 1247–1252.
- (8) Baxter, J. B.; Aydil, E. S. *Appl. Phys. Lett.* **2005**, *86*, 053114.
- (9) Wang, X.; Summers, C. J.; Wang, Z. L. *Nano Lett.* **2004**, *4*, 423–426.
- (10) Gorla, C. R.; Emanetoglu, N. W.; Liang, S.; Mayo, W. E.; Lu, Y.; Wraback, M.; Shen, H. *J. Appl. Phys.* **1999**, *85*, 2595–2602.
- (11) Xu, C.; Xu, G.; Liu, Y.; Wang, G. *Solid State Commun.* **2002**, *122*, 175–179.
- (12) Yao, B. D.; Chan, Y. F.; Wang, N. *Appl. Phys. Lett.* **2002**, *81*, 757–759.

(13) Liu, B.; Zeng, H. C. *J. Am. Chem. Soc.* **2003**, *125*, 4430–4431.

(14) Yang, L.; Wang, G.; Tang, C.; Wang, H.; Zhang, L. *Chem. Phys. Lett.* **2005**, *409*, 337–341.

(15) Xu, L.; Hu, Y.-L.; Pelligra, C.; Chen, C.-H.; Jin, L.; Huang, H.; Sithambaram, S.; Aindow, M.; Joosten, R.; Suib, S. L. *Chem. Mater.* **2009**, *21*, 2875–2885.

(16) Spanhel, L.; Anderson, M. A. *J. Am. Chem. Soc.* **1991**, *113*, 2826–2833.

(17) Tian, Z. R.; Liu, J.; Voigt, J. A.; Mckenzie, B.; Xu, H. *Angew. Chem., Int. Ed.* **2003**, *42*, 413–417.

(18) Du, J.; Liu, Z.; Huang, Y.; Gao, Y.; Han, B.; Li, W.; Yang, G. *J. Cryst. Growth* **2005**, *280*, 126–134.

(19) Guo, L.; Ji, Y. L.; Xu, H.; Simon, P.; Wu, Z. *J. Am. Chem. Soc.* **2002**, *124*, 14864–14865.

(20) Liu, J.; Huang, X.; Li, Y.; Duan, J.; Ai, H. *Mater. Chem. Phys.* **2006**, *98*, 523–527.

(21) Cao, H. L.; Qian, X. F.; Gong, Q.; Du, W. M.; Ma, X. D.; Zhu, Z. K. *Nanotechnology* **2006**, *17*, 3632–3636.

(22) Zhang, J.; Sun, L.; Yin, J.; Su, H.; Liao, C.; Yan, C. *Chem. Mater.* **2002**, *14*, 4172–4177.

(23) Zhang, Y.; Mu, J. *Nanotechnology* **2007**, *18*, 075606.

(24) Zhang, J.; Liu, H.; Wang, Z.; Ming, N. *Appl. Phys. Lett.* **2007**, *90*, 113117.

(25) Zhang, T.; Dong, W.; Keeter-Brewer, M.; Konar, S.; Njabon, R. N.; Tian, Z. R. *J. Am. Chem. Soc.* **2006**, *128*, 10960–10968.

(26) Tian, Z. R.; Voigt, J. A.; Liu, J.; Mckenzie, B.; McDermott, M. J.; Rodriguez, M. A.; Konishi, H.; Xu, H. *Nat. Mater.* **2003**, *2*, 821–826.

shaped ZnO nanostructures largely depends on the relative stability of the crystal faces of the growing nanostructures. Usually, the presence of a capping agent capable of stabilizing a particular crystal facet by adsorption can alter the growth rate in different crystal planes.^{27,28} In this context, several different soft templates/capping agents such as water-soluble polymers,^{31–33} various citrate salts,^{26,28,34} a mixture of sodium citrate and alkylamine,^{25,28} citric acid,³² ethylene diamine,³⁵ water-soluble diblock copolymers,³⁶ surfactants,^{18,19,37} and amino acids³⁸ have been successfully used in wet-chemical methods to tune the size and shape of ZnO nanostructures.

Besides these, there are some other examples of ZnO micro/nanostructure synthesis that are noticeable, for example, the synthesis of hierarchical mesophase ZnO crystals using hybrid organic silane 1,2-bis(trimethoxysilyl)ethane (BTME) along with hexadecyltrimethylammonium chloride (CTAC).¹⁷ Zhang et al. has reported a site-specific sequential nucleation and growth route to synthesize hierarchical complex and oriented ZnO nanostructure.²⁵ Du et al. has reported the synthesis of ZnO nanoflowers in subcritical water in the presence of cetyltrimethylammonium bromide (CTAB) and polyethyleneoxide-polypropyleneoxide-polyethyleneoxide block copolymer (P103) surfactant.¹⁸ In most of these methods of preparing shaped ZnO nanostructures, the externally added surfactants or capping agents were adsorbed preferentially on some crystal planes of the growing particles that ultimately alter the growth kinetics and the relative stability of the crystal faces and hence either promote or inhibit crystal growth in some particular crystal planes, resulting in the formation of anisotropic ZnO nanostructures.^{19,25–28}

Among various applications of ZnO nanostructures, the catalysis/photocatalysis with such nanostructures is the most important one for environmental protection. For example, ZnO has been used for the photodegradation of organic hazards in water³ and for producing sterilized water free of bacteria and pyrogen.³⁹ The photocatalytic activity of ZnO has been extensively studied, but the catalytic activity of ZnO in organic reactions has been poorly studied. There are very few examples where bulk and nanostructured ZnO have been used as catalysts for the Friedel–Crafts acylation of aromatic compounds.^{18,40} The use of ZnO is more advantageous compared to the use of the conventional ZnCl₂ catalyst for such acylation reactions because ZnO is nontoxic, inexpensive, and much less hygroscopic.

In this article, we report a simple wet-chemical approach to the growth of hierarchical ZnO nanostructures of different shapes in the presence of the ascorbate (As) ion at relatively low

temperature. We have varied different reaction parameters such as the concentration of the reactant and the shape-directing agent, the pH, and the reaction temperature to study their effect on the size and shape of the formed hierarchical ZnO nanostructures. Ascorbic acid (AA) is a natural sugar acid with good antioxidant properties, and it generally exhibits keto–enol tautomerism, of which the enol form is susceptible to ionization in aqueous solution. Thus, it can be easily converted to its mineral salts by treating with mineral carbonates or hydroxides. Ascorbic acid or mineral ascorbate is very reactive and has been used as a versatile reducing-cum-shape-directing agent for preparing metal NPs.⁴¹ Thus, we feel that it is important to investigate the aqueous phase synthesis of ZnO nanostructures of various shapes using the biodegradable “green” ascorbic acid molecule as a capping agent. A detailed survey of the literature shows that compared to other-shaped ZnO nanostructures there exist only a few reports on the preparation of hierarchical ZnO nanostructures that are somewhat flowerlike in appearance by wet-chemical methods.^{38,42–51} For example, Zhang et al. have reported the preparation of ZnO nanostructures of flower-, rod-, and prism-shaped morphology by decomposing the zinc precursors at higher temperature.²² Liu et al. have synthesized ZnO nanoflowers by the alkaline hydrolysis of zinc nitrate using ammonium hydroxide.^{20,42} An array of multineedle-shaped ZnO nanostructures, whose individual particle morphology is closer to that of a flower, have also been prepared by Masuda et al.⁵² using site-selective deposition techniques. Du et al. also synthesized flowerlike ZnO on the surfaces of multiwalled carbon nanotubes.⁴⁴ However, a systematic study of the morphology evolution to provide insight into the formation mechanism of such flowerlike ZnO nanostructures has not yet been reported. Moreover, the obtained shape of ZnO nanostructures by our method is different from those reported by other researchers mentioned above. We have also performed some control experiments to elucidate the detailed mechanism of the formation of these flowerlike ZnO nanostructures. First, the time-dependent morphology evolution process (at 60 and 30 °C) was examined via field-emission scanning electron microscopy (FESEM) and transmission electron microscopy (TEM). These results revealed that flowerlike ZnO nanostructures (microcrystals) are composed of small spherical nanocrystallites (~20–30 nm). We have also systematically optimized the growth condition by manipulating the reactant concentration as well as the additional reactant addition. This process yields spherical nanocrystallites and spindlelike nanostructures as primary and secondary structures, which are intermediates on the pathway of formation of large flowerlike nanostructures. Moreover, we have also isolated the different intermediate shapes, such as

- (27) Tian, Z. R.; Voigt, J. A.; Liu, J.; Mckenzie, B.; Mcdermott, M. J. *J. Am. Chem. Soc.* **2002**, *124*, 12954–12955.
 (28) Sounart, T. L.; Liu, J.; Voigt, J. A.; Huo, M.; Spoerke, E. D.; Mckenzie, B. *J. Am. Chem. Soc.* **2007**, *129*, 15786–15793.
 (29) Pacholski, C.; Kornowski, A.; Weller, H. *Angew. Chem., Int. Ed.* **2002**, *41*, 1188–1191.
 (30) Wu, X.; Jiang, P.; Cai, W.; Bai, X.-D.; Gao, P.; Xie, S.-S. *Adv. Eng. Mater.* **2008**, *10*, 476–481.
 (31) Muoz-Espi, R.; Jeschke, G.; Lieberwirth, I.; Gmez, C. M.; Wegner, G. *J. Phys. Chem. B* **2007**, *111*, 697–707.
 (32) Zhang, H.; Yang, D.; Li, D.; Ma, X.; Li, S.; Que, D. *Cryst. Growth Des.* **2005**, *5*, 547–550.
 (33) Rashid, M. H.; Raula, M.; Bhattacharjee, R. R.; Mandal, T. K. *J. Colloid Interface Sci.* **2009**, *339*, 249–258.
 (34) Cho, S.; Jang, J.; Jung, S.; Lee, B. R.; Oh, E.; Lee, K. *Langmuir* **2009**, *25*, 3825–3831.
 (35) Pal, U.; Santiago, P. *J. Phys. Chem. B* **2005**, *109*, 15317–15321.
 (36) Taubert, A.; Glasser, G.; Palms, D. *Langmuir* **2002**, *18*, 4488–4494.
 (37) Zhang, X. L.; Qiao, R.; Qiu, R.; Kim, J. C.; Kang, Y. S. *Cryst. Growth Des.* **2009**, *9*, 2906–2910.
 (38) Umetsu, M.; Mizuta, M.; Tsumoto, K.; Ohara, S.; Takami, S.; Watanabe, H.; Kumagai, I.; Adscharina, T. *Adv. Mater.* **2005**, *17*, 2571–2575.
 (39) Sato, K.; Aoki, M.; Noyori, R. *Science* **1998**, *281*, 1646.
 (40) Sarvari, M. H.; Sharghi, H. *J. Org. Chem.* **2004**, *69*, 6953–6956.

- (41) Dinda, E.; Si, S.; Kotal, A.; Mandal, T. K. *Chem.—Eur. J.* **2008**, *14*, 5528–5537.
 (42) Liu, J.; Huang, X.; Li, Y.; Duan, J.; Ai, H.; Ren, L. *Mater. Sci. Eng., B* **2006**, *127*, 85–90.
 (43) Wang, J.; Cao, J.; Fang, B.; Lu, P.; Deng, S.; Wang, H. *Mater. Lett.* **2005**, *59*, 1405–1408.
 (44) Du, Y.; Hao, C.; Wang, G. *Mater. Lett.* **2008**, *62*, 30–32.
 (45) Yu, S.; Wang, C.; Yu, J.; Shi, W.; Deng, R.; Zhang, H. *Nanotechnology* **2006**, *17*, 3607–3612.
 (46) Gao, Y.-F.; Miao, H.-Y.; Luo, H.-J.; Nagai, M. *Cryst. Growth Des.* **2008**, *8*, 2187–2193.
 (47) Jung, J. Y.; Park, N.-K.; Han, S.-Y.; Han, G. B.; Lee, T. J.; Ryu, S. O.; Chang, C.-H. *Curr. Appl. Phys.* **2008**, *8*, 720–724.
 (48) Ahsanulhaq, Q.; Kim, S. H.; Kim, J. H.; Hahn, Y. B. *Mater. Res. Bull.* **2008**, *43*, 3483–3489.
 (49) Li, P.; Liu, H.; Zhang, Y.-F.; Wei, Y.; Wang, X.-K. *Mater. Chem. Phys.* **2007**, *106*, 63–69.
 (50) Gao, X.; Li, X.; Yu, W. *J. Phys. Chem. B* **2005**, *109*, 1155–1161.
 (51) Richardson, J. J.; Lange, F. F. *Cryst. Growth Des.* **2009**, *9*, 2570–2575.
 (52) Masuda, Y.; Kinoshita, N.; Sato, F.; Koumoto, K. *Cryst. Growth Des.* **2006**, *6*, 75–78.

Table 1. Reaction Recipe for the Preparation of ZnO Nanostructures and Their Characterization Data^a

sample name	[ZnAc ₂] (M)	[NaOH] (M)	[NaAs] (M)	yield (%)	shape	pH	size ^b (nm)	<i>R</i> _{(002)/(101)} ^d
ZnO/As-1	0.01	0.05	0.001	100	flower	12.0	600–800	0.75
ZnO/As-2	0.01	0.05	0.005	100	flower	12.0	800–950	0.76
ZnO/As-3	0.01	0.05	0.01	100	flower	12.0	1000–1200	0.78
ZnO/As-4	0.004	0.05	0.001	100	flower	12.5	^c	0.77
ZnO/As-5	0.004	0.05	0.01	100	flower	12.5	^c	0.83
ZnO-6	0.01	0.05		100	irregular	12.0		0.66

^a Temperature = 60 °C. Time = 30 min. ^b Sizes (maximum end-to-end distance between the opposite petals of a flower) were determined from FESEM pictures (particle count = 25). ^c Unable to determine. ^d Measured intensity ratio of the peaks corresponding to planes (002) and (101), obtained from the powder XRD pattern.

flower (at 60 °C), spindle (at 70 °C), spindle and sphere mixture (at 80 °C), and sphere (at 90 °C), during the temperature-dependent shape evaluation study. This type of morphological study on ZnO nanostructures has not been reported very often by other researchers. We also examined the optical properties of the as-synthesized differently shaped ZnO nanostructures. Again, flowerlike ZnO nanostructures are supposed to have a high surface-to-volume ratio. It has been reported that the flowerlike nanostructures of materials (e.g., TiO₂, gold, iron oxide, etc.) are catalytically more active than their spherical counterparts because of their higher surface area.^{53–56} This prompted us to use flowerlike ZnO as a catalyst in the Friedel–Crafts acylation of anthracene with benzoyl chloride. The catalytic activity of flowerlike and spherical ZnO nanostructures in this reaction has also been compared.

Experimental Section

Materials. Zinc acetate (ZnAc₂) dihydrate, zinc nitrate hexahydrate, zinc sulfate heptahydrate, and sodium hydroxide were purchased from Merck (India). Ascorbic acid (AA) and trisodium citrate dihydrate were purchased from Aldrich and SRL (India), respectively. Anthracene, benzoyl chloride, tyrosine, and tartaric acid were purchased from Spectrochem (India). Benzoyl chloride was vacuum distilled prior to use. Dichloromethane (CH₂Cl₂) and sodium bicarbonate were purchased from Merck (India). *d*₆-DMSO, D₂O, and CDCl₃ were purchased from Aldrich. All chemicals were used as received. Triply distilled water was used as a reaction medium.

Preparation of Sodium Ascorbate (NaAs). The sodium salt of ascorbic acid (NaAs) was prepared by neutralizing aqueous ascorbic acid (AA) with sodium hydroxide solution at pH 7 using a pH meter. The resultant solution was then freeze dried to isolate the solid NaAs, which was characterized with NMR and FTIR spectroscopy (details in Supporting Information, SI). Similarly, sodium tartarate and sodium tyrosinate were also synthesized (details in SI).

Synthesis of Ascorbic Acid-Based Ionic Liquids. Two different ascorbic acid-based ionic liquids, 1-ethyl-3-methylimidazolium ascorbate ([C₂mim][As]) and 1-hexyl-3-methylimidazolium ascorbate ([C₆mim][As]) were synthesized and characterized by following the procedure described in our earlier report.⁴¹

Synthesis of Hierarchical ZnO Nanostructures with Flowerlike Morphology. Two different sets of reactions were mainly carried out for the preparation of flowerlike ZnO nanostructures. In the first set, the molar ratio of NaOH to zinc acetate (ZnAc₂) was set to 5:1 with [ZnAc₂] = 0.01 M, and in the second set, this ratio was set to 12.5:1 with [ZnAc₂] = 0.004 M. The only parameter that was systematically varied in both sets was the

Table 2. Preparation of ZnO Nanostructures at Different pH Values and Their Characterization Data^a

sample name	[NaOH] (M)	pH	[NaAs] (M)	yields (%)	shape
ZnO/As-7	0.03	10	0.001	~90	flower
ZnO/As-8	0.1	14	0.001	100	flower
ZnO-9	0.03	10			mixed morphology
ZnO-10	0.1	14			no defined morphology

^a [ZnAc₂] = 0.01 M. Temperature = 60 °C. Time = 30 min.

concentration of NaAs, which was changed from 0 to 0.01 M (details in Table 1). In a typical synthesis of flowerlike ZnO nanostructure, 5 mL of aqueous NaOH (0.5 M) solution was added dropwise to a stirring mixture of 5 mL of ZnAc₂ (0.1 M), 5 mL of NaAs (0.01 M), and 35 mL of water preheated to 60 °C. The reaction mixture was then heated for another 30 min at the same temperature and then allowed to cool to room temperature under constant magnetic stirring. The white suspension was then centrifuged at 21000g for 30 min to isolate the product. The collected white mass was purified from any trace of unreacted materials by two cycles of washing with water, redispersion, and centrifugation. Finally, the collected product was dried under vacuum at 60 °C for 24 h. This set of reactions was labeled ZnO/As-1 (details in Table 1). The purified, dried powder ZnO samples were used for microscopy, FTIR spectroscopy, and diffractometric analysis. A few more sets of reactions were also performed by varying the pH of the reaction medium (Table 2) and the reaction temperature (Table 3) to investigate their effects on the shape and size of the formed ZnO nanostructures.

Friedel–Crafts Acylation of Anthracene with ZnO Nanostructures. The acylation reaction of anthracene was carried out using purified ZnO nanostructures as a catalyst without any further surface modification following the method reported earlier by Sarvari et al.⁴⁰ Typically, a mixture of anthracene (1 mmol) and the desired number of ZnO nanostructures (sample ZnO/As-1) (Table 5) were placed in a round-bottomed flask and mixed thoroughly under magnetic stirring. To this reaction mixture, benzoyl chloride (2 mmol) was then added, which immediately resulted in the color change of the reaction mixture from white to deep blue. The progress of the reaction was then monitored via thin-layer chromatography (TLC) by withdrawing an appropriate amount of the reaction mixture. Stirring was continued for 2 h at room temperature, after which the reaction was complete. After the completion of the reaction, the reaction mixture was stirred with dichloromethane and ZnO was removed by filtration. Finally, the eluted dichloromethane part was washed four or five times with an aqueous solution of sodium bicarbonate and dried over anhydrous sodium sulfate. Finally, the product along with the unreacted starting reactants was isolated by solvent evaporation. The yield of the product was calculated using ¹H NMR spectroscopy in CDCl₃. The crude product was purified using silica-gel column chromatography (100–200 mesh) using petroleum ether initially to remove the starting materials and then 20% ethyl acetate in petroleum ether

(53) Wu, G.; Wang, J.; Thomas, D. F.; Chen, A. *Langmuir* **2008**, *24*, 3503–3509.

(54) Zheng, Y.; Cheng, Y.; Wang, Y.; Bao, F.; Zhou, L.; Wei, X.; Zhang, Y.; Zheng, Q. *J. Phys. Chem. B* **2006**, *110*, 3093–3097.

(55) Li, M.; Zhao, G.; Geng, R.; Hu, H. *Bioelectrochemistry* **2008**, *74*, 217–221.

(56) Firooz, A. A.; Mahjoub, A. R.; Khodadadi, A. A. *Mater. Chem. Phys.* **2009**, *115*, 196–199.

Table 3. Preparation of ZnO Nanostructures at Different Reaction Temperatures and Their Characterization Data^a

sample name	temperature (°C)	morphology	size (nm) ^b	$R_{(002)/(101)}$
ZnO/As-11	30	flower	800–1000 ^c	0.95
ZnO/As-1	60	flower	600–800	0.75
ZnO/As-12	70	spindle	450–600 ^d	0.68
ZnO/As-13	80	spindle and spherical	250–400 ^c and 200–300 ^e	0.64
ZnO/As-14	90	spherical	130–180 ^e	0.67

^a Conditions: similar to that used for sample ZnO/As-1 in Table 1. ^b Sizes were determined from the FESEM pictures (particle count = 25) similarly to sizes obtained in Table 1. ^c Maximum end-to-end distance between two exactly opposite petals of a ZnO flower. ^d Maximum end-to-end distance (length) of the spindlelike ZnO. ^e Maximum diameter of the spherical ZnO particle.

to elute the product. The ¹H NMR spectral analysis data of the product, 9-benzylanthracene, is given as follows: ¹H NMR [300 MHz; CDCl₃; TMS] δ 8.58 (s, 1H, Ha), 8.06–8.13 (m, 2H, Hb *J* = 8.4 Hz), 7.81–7.84 (d, 2H, Hc *J* = 7.8 Hz), 7.71–7.74 (d, 2H, Hd *J* = 8.7 Hz), 7.37–7.61 (m, 7H, He).

Characterization. For FESEM studies, the powder ZnO samples were spread onto copper tape supported on a metal stub and sputter coated with platinum to minimize charging. The images were then recorded by placing the sample under a JEOL JSM-6700F electron microscope operated at an accelerating voltage of 5 kV. Energy-dispersive X-ray (EDX) spectroscopic measurements were performed via the same instrument.

The crystallinity of the purified dried nanostructured ZnO powders was studied using a Bruker D8 X-ray diffractometer operated at an accelerating voltage of 40 kV with a current intensity of 40 mA.

FTIR spectra of NaAs and the purified dried ZnO powders were recorded using KBr pellets in a Nicolet Magna-750 spectrophotometer. The pellets were prepared by mixing the corresponding dried sample with KBr in a 1:100 (w/w) ratio.

For high-resolution TEM measurements, one drop of the aqueous redispersed suspension of ZnO nanostructures was placed on a carbon-coated copper grid and allowed to dry in air. The grid was then observed on a JEOL JEM-2010 electron microscope operated at an accelerating voltage of 200 kV.

UV-visible absorption spectra of an aqueous suspension of ZnO nanostructures were recorded using a Hewlett-Packard 8453 spectrophotometer by transferring an appropriate volume of the ZnO suspension to a quartz cuvette.

The PL spectra of an aqueous suspension of ZnO nanostructures were recorded using a Jobin-Yvon Fluoromax-3 photoluminescence spectrophotometer. For PL measurement, the samples' water suspensions were excited at a wavelength of 340 nm.

All ¹H NMR studies of the organic compounds were carried out with a Bruker DPX 300 MHz spectrometer, and the spectra are available in the Supporting Information.

Results and Discussion

Synthesis of Hierarchical ZnO Nanostructures. Nanostructured ZnO flowers were prepared by the simple hydrolysis of zinc acetate (ZnAc₂) with aqueous NaOH in the presence of the ascorbate (As) ion as a shape-directing/capping agent at relatively low temperature (ca. 60 °C) as described in the Experimental Section. Tables 1 and 2 illustrate the various reaction conditions and the detailed recipes for the synthesis of flowerlike ZnO nanostructures. The presence of ascorbate could guarantee the controlled growth of flowerlike ZnO crystals. The data also reveal that the yields of ZnO nanostructures in these reactions with ascorbate are almost 100% within just 30 min of reaction. Similar reactions were also carried out in the presence of other capping agents such as ascorbic acid, sodium citrate, sodium tartarate, and sodium tyrosinate instead of sodium ascorbate to investigate the effect of the nature of the additives on the morphology of the formed ZnO nanostructures. The obtained ZnO nanostructures were examined via FESEM, TEM, and X-ray diffractometry (XRD) techniques, which will be discussed later in this section.

Field-Emission Scanning Electron Microscopy (FESEM).

The morphologies of the as-synthesized ZnO nanostructures, prepared under different reaction conditions according to Table 1, were primarily examined through FESEM. Figure 1A shows the FESEM image of the ZnO/As-1 sample prepared at a molar ratio of [ZnAc₂]/[NaOH]/[ascorbate] = 1:5:0.1 at a solution pH of 12 (Table 1). The image clearly shows the formation of well-defined flowerlike ZnO nanostructures. These flowerlike ZnO nanostructures are very uniform and polydisperse in nature. It is interesting that we did not observe any other morphology rather than flower. It should be noted that the morphology of these ZnO nanostructures is quite different from those reported earlier, although all of them are named flowerlike nanostructures.^{20,22} Furthermore, the ZnO/As-2 and ZnO/As-3 samples (Table 1) prepared with 5 and 10 times higher ascorbate concentrations than used for sample ZnO/As-1 and with [ZnAc₂]/[NaOH]/[ascorbate] molar ratios of 1:5:0.5 and 1:5:1 also have similar flowerlike morphology (Figure 1B,C, respectively). The enlarged view of a flowerlike ZnO provided in the insets of Figure 1A–C clearly indicates that these nanostructures more or less resemble a flower bud. This flower bud actually consists of a central half-spindle and a few half-spindles pointing outward that look like the petals of a flower initiating from the center of the half-spindle. The average sizes (maximum end-to-end distance between two exactly opposite petals) of these flowerlike ZnO's are varied from 600 to 800 nm for sample ZnO/As-1, from 800 to 950 nm for sample ZnO/As-2, and from 1000 to 1200 nm for sample ZnO/As-3.

It is known that the concentration of the zinc precursor plays a crucial role in controlling the shape and size of ZnO nanostructures. To determine whether there is any effect of metal precursor concentration in our case, we repeated the experiments by lowering the concentration of ZnAc₂ from 0.01 to 0.004 M and the rest of the conditions were similar to those used for samples ZnO/As-1 and ZnO/As-3 (Table 1). The formed ZnO nanostructures were designated as ZnO/As-4 and ZnO/As-5. The FESEM images of these two samples (ZnO/As-4 and ZnO/As-5) again show the formation of flowerlike ZnO nanostructures (Figure 1D,E, respectively). In these cases, we are unable to measure the size ranges of these ZnO nanostructures because we are not able to locate a considerable number of flowers (around 25) because of their overlapping fashion, as can be seen in the FESEM images (Figure 1D,E). However, it is possible to measure the end-to-end distance between the opposite petals of a typical flower, as shown in the insets of Figure 1C,D, which is about 760 nm for sample ZnO/As-4 and 820 nm for sample ZnO/As-5. In these cases, the pH of the reaction medium was measured to be 12.5, which is nearly the same as that (pH 12) measured for samples ZnO/As-1 and ZnO/As-3 (Table 1). Therefore, in the last two cases, one should not expect any effect of the medium pH on the formation of such flowerlike ZnO nanostructures. Thus, it may be concluded that flowerlike ZnO nanostructures are formed over a wide range of zinc precursor concentration (ca. 0.004–0.01 M).

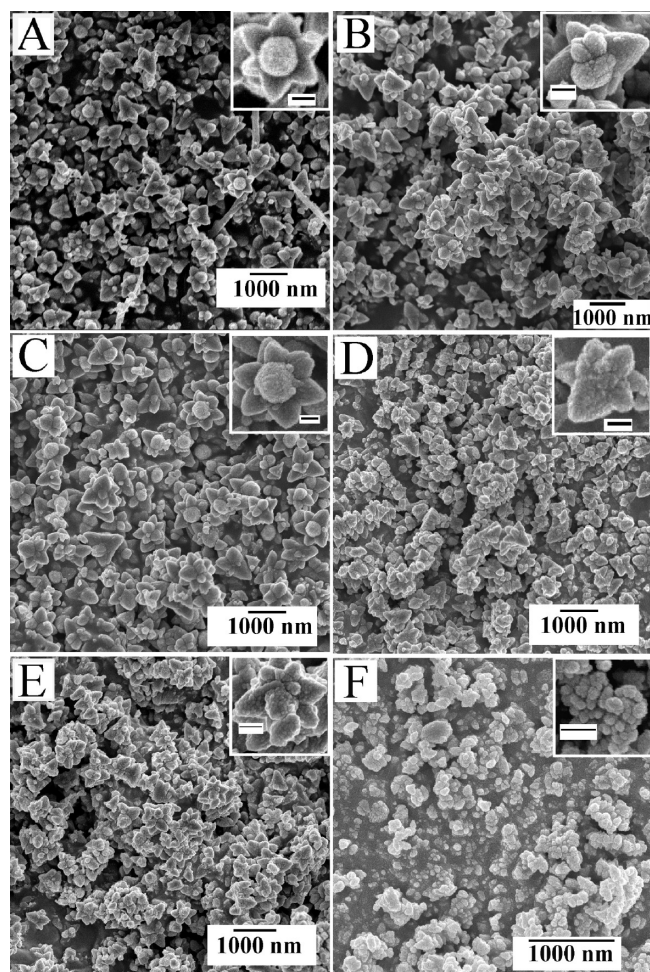


Figure 1. FESEM images of different ZnO nanostructure samples prepared under different conditions as mentioned in Table 1: (A) ZnO/As-1, (B) ZnO/As-2, (C) ZnO/As-3, (D) ZnO/As-4, (E) ZnO/As-5, and (F) ZnO-6. (Insets) Enlarged views of the corresponding images; scale bars are 200 nm.

To study the effect of ascorbate on the morphology, we prepared sample ZnO-6 in the absence of ascorbate under reaction conditions similar to that used for sample ZnO/As-1. Interestingly, we did not observe any regular flowerlike morphology via FESEM (Figure 1F) of this sample (ZnO-6); rather, some aggregated structures with undefined morphologies were observed. Upon comparison of FESEM images provided in Figure 1, it is clear that the flowerlike ZnO nanostructures are formed only in the presence of ascorbate. It seems that the concentration of ascorbate does not have any effect on the shape of ZnO; rather, the average size of the flowerlike ZnO nanostructures increases with increasing ascorbate concentration in the reaction medium. Thus, the presence of ascorbate ions in the reaction medium induces the growth of ZnO in a particular direction that ultimately results in the formation of such anisotropic flowerlike morphology.

Again, it is also known that the pH of the reaction medium is a vital parameter for controlling the shape of ZnO nanostructures when the other parameter remains unaltered.^{23,28} To check this issue in our system, we also performed two more sets of reactions (samples ZnO/As-7 and ZnO/As-8 in Table 2) by varying the concentration of NaOH and keeping all other reaction parameters the same as used for sample ZnO/As-1 (Table 1). The FESEM image (Figure 2A) of sample ZnO/As-7, prepared at

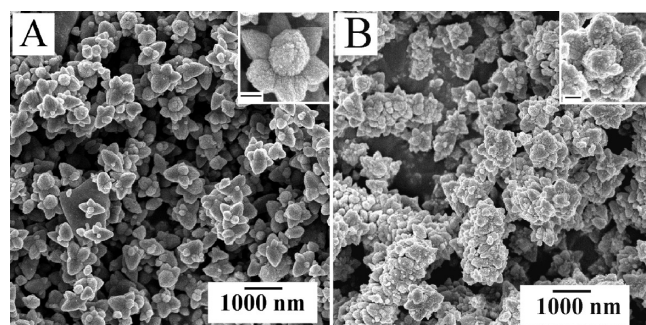


Figure 2. FESEM images of different ZnO nanostructure samples prepared at reaction medium pH values of ~ 10 and 14 (Table 2): (A) ZnO/As-7 and (B) ZnO/As-8. (Insets) Enlarged views of the corresponding images; scale bars = 200 nm.

pH 10, again shows flowerlike ZnO nanostructures that are similar in morphology to that observed for sample ZnO/As-1 (Figure 1A), prepared at pH 12. When the concentration of NaOH is increased to 0.1 M (pH ~ 14), the FESEM image of sample ZnO/As-8 (Figure 2B) again shows flowerlike morphology. However, there are some particles on the surface of the petals of this flowerlike ZnO, as can also be seen in the magnified image of a single ZnO nanostructure shown in the inset of Figure 2B. At this point, we do not know the exact reason for the formation of such particles. However, one possible reason for the concentration of NaOH being higher than that used for the preparation of samples ZnO/As-1 and ZnO/As-7 is that the rate of reaction is higher, which may result in the formation of such particles. Thus, it may be concluded that flowerlike ZnO nanostructures are formed over a wide range of pH (ca. 10–14).

Similar to the earlier cases, we have also prepared ZnO nanostructures in the absence of ascorbate (samples ZnO-9 and ZnO-10) by maintaining reaction conditions similar to that maintained for samples ZnO/As-7 and ZnO/As-8, respectively (Table 2). The FESEM images of these samples exhibit some undefined morphologies (Figure S1 in SI). These results further confirm that the presence of the ascorbate ion is absolutely necessary for obtaining flowerlike nanostructures, no matter what the pH of the reaction medium.

In any nanostructure synthesis, the reaction temperature is another key parameter whose manipulation can affect the final shape of the formed nanostructures. To determine the effect of reaction temperature in the present case, we performed four different set of reactions under conditions similar to those used for sample ZnO/As-1 in Table 1 but at four different temperatures (30, 70, 80, and 90 °C). The resulting ZnO samples are designated as ZnO/As-11, ZnO/As-12, ZnO/As-13, and ZnO/As-14, respectively (Table 3). Sample ZnO/As-11 prepared at 30 °C (Figure 3A) again shows the formation of flowerlike nanostructures similar to those observed for sample ZnO/As-1, prepared at 60 °C (cf. Figures 1A and 3A). However, the sizes (maximum end-to-end distance between two exactly opposite petals) of flowerlike ZnO nanostructures (sample ZnO/As-11) prepared at 30 °C (800–1000 nm) are larger than that (sample ZnO/As-1) prepared at 60 °C. Also, the number of petals in a single flower is greater than that observed in a sample prepared at 60 °C (cf. Figures 1A and 3A). When the reaction temperature was increased from 60 to 70 °C, the FESEM image of the obtained ZnO/As-12 sample (Figure 3B) shows distorted flowerlike morphology along with some spindlelike morphology with some kind of debris on it. The width and length of these spindles are in the ranges of 300–400 and 450–600 nm, respectively. However, when the

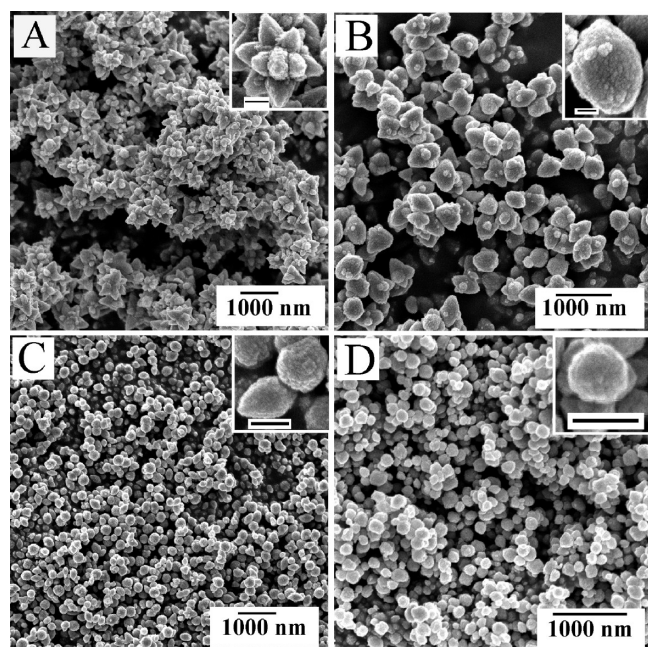


Figure 3. FESEM images of different ZnO nanostructure samples prepared at different reaction temperatures (Table 3): (A) ZnO/As-11 at 30 °C, (B) ZnO/As-12 at 70 °C, (C) ZnO/As-13 at 80 °C, and (D) ZnO/As-14 at 90 °C. (Insets) Enlarged views of the corresponding images; scale bars = 200 nm.

sample (ZnO/As-13 in Table 3) was prepared at 80 °C, a mixture of spherical- and spindle-shaped ZnO nanostructures having sizes of about 250–400 and 200–300 nm, respectively, was obtained (Figure 3C). Note that we do not observe the formation of any flowerlike ZnO nanostructures at this temperature. Further increases in the reaction temperature to 90 °C resulted in the formation of only spherical ZnO NPs in sample ZnO/As-14, as can be seen from the corresponding FESEM image provided in Figure 3D. The average diameter of these spherical ZnO NPs is around 130–180 nm. These results indicate that besides the presence of ascorbate, the reaction temperature also plays a major role in determining the final shape of ZnO nanostructures. This is due to the fact that at low temperatures the ascorbate ion prefers to absorb onto the reactive planes of ZnO (usually the (001) plane),^{26,34,57} lowering the activation energy needed for nucleation and crystal growth and directing the formation of branches. When the temperature is 90 °C, all surface planes have gained enough activation energy for nucleation and crystal growth, leading to the formation of isotropic spherical particles.⁵⁸ The adsorption of ascorbate onto the ZnO surface was confirmed via FTIR spectroscopy, which will be discussed in detail later in this section. Also, the issue of the adsorption of ascorbate preferentially onto the (001) plane will also be discussed in detail later in this section. Consequently, we have observed the formation of spindle-shaped nanostructures at 70 °C and spherical particles at even higher temperature. Earlier, Cheon et al. also reported a similar type of temperature-dependent shape transformation from multipods to thermodynamically favorable truncated octahedrons in the case of PbS nanostructures.⁵⁸ They have also been able to identify the intermediate states, such as stars at intermediate temperature. The same group has also reported a similar type of observation in the case of MnS NPs, where rod-shaped

morphology was transformed to spherical and cube morphology at higher temperature.⁵⁹ By utilizing this concept, we can assume that at lower temperature with a high flux of reactants (zinc precursor, NaOH, and ascorbate), kinetically controlled growth might take place, favoring anisotropic ZnO nanostructures.⁶⁰

To study the effect of the nature of additives, we have performed some additional experiments. First, we have synthesized ZnO nanostructures in the presence of neat ascorbic acid (AA) and two ascorbate ion-based ionic liquids such as 1-ethyl-3-methylimidazolium ascorbate ($[C_2mim][As]$) and 1-hexyl-3-methylimidazolium ascorbate ($[C_6mim][As]$) instead of sodium ascorbate (NaAs) under reaction conditions similar to those used for sample ZnO/As-1. The FESEM images show the formation of only flowerlike ZnO nanostructures (Figure 4). However, these ZnO flowers are relatively larger than those observed for sample ZnO/As-1 prepared in the presence of NaAs. These results further prove that the presence of the ascorbate ion is essential for the growth of such flowerlike ZnO nanostructures. It is worth mentioning that in this synthesis one can use neat ascorbic acid rather than NaAs. However, for easy pH adjustment, we have used NaAs instead of AA. As mentioned in the Introduction, we used these ionic liquids as a reducing-cum-shape-directing agent for the generation of anisotropic gold nanostructures.⁴¹ Besides AA and its different salts, we have also prepared ZnO nanostructures in the presence of similar kinds of other additives such as sodium citrate, sodium tartarate, tyrosine, and sodium tyrosinate. Surprisingly, we observe the formation of flowerlike morphology with the use of sodium citrate additive only (Figure 5A), but the FESEM images of ZnO nanostructures prepared with other additives such as sodium tartarate, tyrosine, and sodium tyrosinate show different morphology than such flowers (Figure 5B–D).

To determine whether the nature of the zinc precursor affects the final morphology, we prepared ZnO from zinc nitrate instead of $ZnAc_2$, keeping the rest of the parameters similar to those used for sample ZnO/As-1. The FESEM image of this sample shows solely flowerlike morphology (Figure 6A). Furthermore, the hydrolysis of $ZnAc_2$ with NH_4OH instead of NaOH under reaction conditions similar to those used for ZnO/As-1 also produces flowerlike ZnO nanostructures as confirmed by FESEM analysis (Figure 6B). It seems that the flowers prepared using NH_4OH are somewhat larger than the flowers observed for sample ZnO/As-1 prepared with NaOH (cf. Figures 1A and 6B). On the basis of these FESEM results, it is very clear that the ascorbate ion plays a key role in determining the shape of the ZnO nanostructures. During the growth of ZnO, the ascorbate ion might be adsorbed on some specific crystal planes of the growing ZnO and thereby alter the growth rate in a different crystal plane, resulting in the formation of flowerlike nanostructures. The adsorption of ascorbate on the surface of ZnO was confirmed via FTIR spectroscopy, which will be discussed later in this section. Earlier, several research groups also observed a similar effect of capping agents on the shape evolution of ZnO nanostructures.^{17,19,25–28} In our case, a probable mechanism for the growth of ZnO nanostructures will be discussed in detail later in this section on the basis of some control experiments.

X-ray Diffraction. The purity and crystalline properties of the formed ZnO nanostructures were examined via powder X-ray diffraction (XRD). Figures 7 and 8 shows the XRD patterns of different ZnO samples prepared under different

(57) Yang, H. G.; Sun, C. H.; Qiao, S. Z.; Zou, J.; Liu, G.; Smith, S. C.; Cheng, H. M.; Lu, G. Q. *Nature* **2008**, *453*, 638–641.

(58) Lee, S.-M.; Jun, Y.-W.; Cho, S.-N.; Cheon, J. *J. Am. Chem. Soc.* **2002**, *124*, 11244–11245.

(59) Jun, Y.-W.; Jung, Y.-Y.; Cheon, J. *J. Am. Chem. Soc.* **2002**, *124*, 615–619.

(60) Jun, Y.-W.; Choi, J.-S.; Cheon, J. *Angew. Chem., Int. Ed.* **2006**, *45*, 3414–3439.

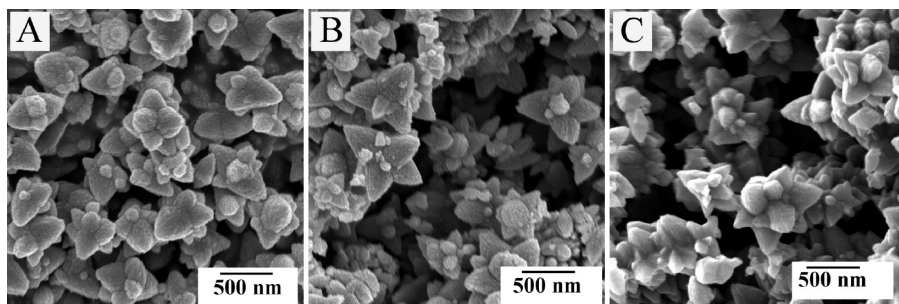


Figure 4. FESEM images of ZnO nanostructures prepared using different capping agents: (A) ascorbic acid, (B) 1-ethyl-3-methylimidazolium ascorbate, and (C) 1-hexyl-3-methylimidazolium ascorbate. The other reaction conditions were similar to those used for sample ZnO/As-1.

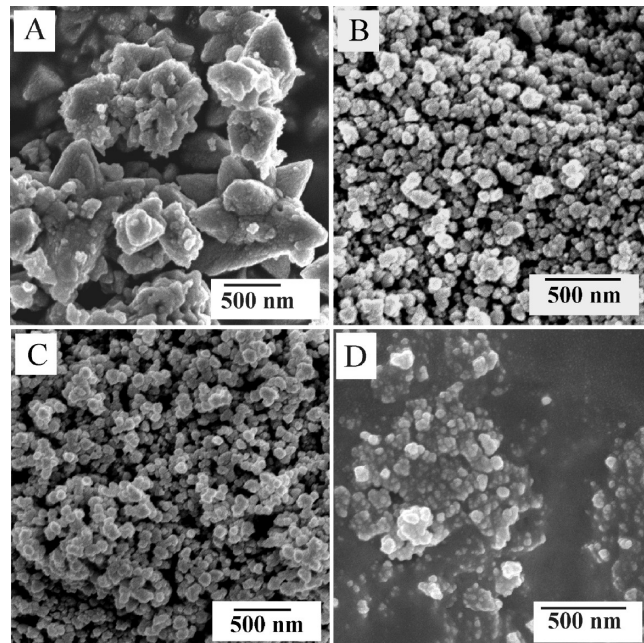


Figure 5. FESEM images of ZnO nanostructures prepared in the presence of different capping agents: (A) sodium citrate, (B) sodium tartarate, (C) tyrosine, and (D) sodium tyrosinate. The samples were prepared according to reaction conditions similar to those used for sample ZnO/As-1.

reaction conditions. The diffraction peaks observed at $2\theta = 31.8$, 34.5, 36.4, 47.5, 57.1, 63.2, 66.7, 67.8, 69, 72.6, and 76.8° for all of the samples presented in Tables 1 and 3 match that of bulk wurtzite hexagonal ZnO having lattice constants of a and c equal to 3.25 and 5.21 Å, respectively (JCPDS file no. 36-1451). Note that no characteristic peaks corresponding to impurities, such as zinc hydroxide, were observed in the XRD patterns of any of the samples that indicated the formation of pure ZnO nanostructures. The measured intensity ratio, $R_{(002)/(101)}$, of the peaks belonging to the (002) and (101) planes for all of the samples are depicted in Tables 1 and 3. The values of $R_{(002)/(101)}$ are 0.75, 0.76, 0.78, 0.77, and 0.83 for samples ZnO/As-1 (Figure 7a), ZnO/As-2 (Figure 7b), ZnO/As-3 (Figure 7c), ZnO/As-4 (Figure 7d), and ZnO/As-5 (Figure 7e), respectively. The measured intensity ratio, $R_{(002)/(101)}$, for sample ZnO-6 (Figure 7f) prepared in the absence of ascorbate is 0.66. These values of $R_{(002)/(101)}$ for all of the samples with flower-like morphology are higher than that (0.66) of sample (ZnO-6) without flowerlike morphology. Moreover, these values are much higher than the corresponding standard value of 0.44 of bulk hexagonal wurtzite ZnO. It could also be noted that the value of $R_{(002)/(101)}$ increases as the samples are prepared with increasing ascorbate concentration in the reaction medium (Table 1).

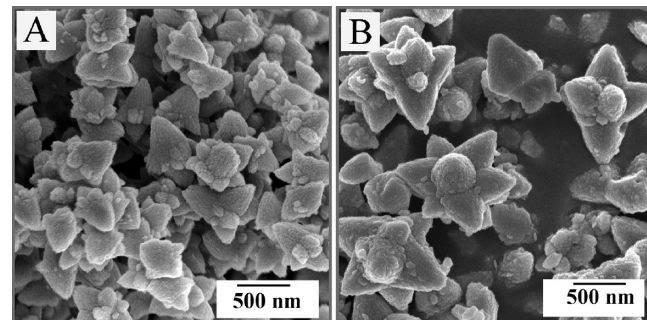


Figure 6. FESEM images of ZnO nanostructures prepared from (A) zinc nitrate under reaction conditions similar to those used for sample ZnO/As-1 (i.e., $[Zn^{2+}] = 0.01$ M, $[NaOH] = 0.05$ M, and $[NaAs] = 0.001$ M). (B) $ZnAc_2$ using NH_4OH at $[Zn^{2+}] = 0.01$ M, $[NH_4OH] = 0.05$ M, and $[NaAs] = 0.001$ M.

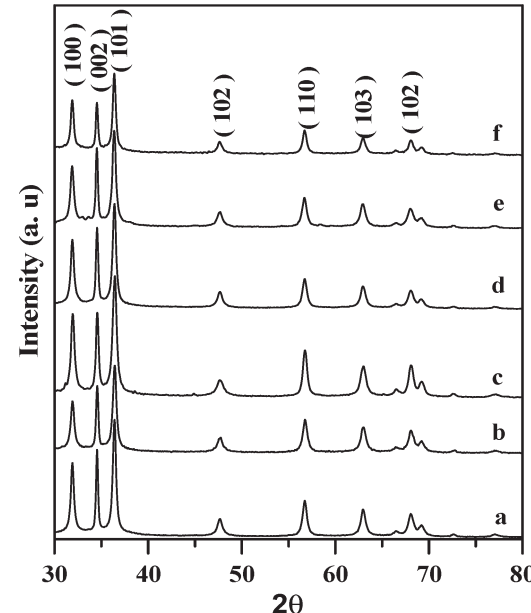


Figure 7. XRD patterns of different hierarchical ZnO nanostructured samples from Table 1: (a) ZnO/As-1, (b) ZnO/As-2, (c) ZnO/As-3, (d) ZnO/As-4, (e) ZnO/As-5, and (f) ZnO-6.

The XRD patterns of samples ZnO/As-11, ZnO/As-1, ZnO/As-12, ZnO/As-13, and ZnO/As-14 prepared at temperatures of 30, 60, 70, 80, and 90 °C, respectively, again exhibit all of the peaks corresponding to wurtzite hexagonal ZnO (Figure 8). However, the values of $R_{(002)/(101)}$, as depicted in Table 3, decrease as the shape of ZnO nanostructures transforms from flower to spindle to sphere. From these results, in brief, it may be concluded that in the

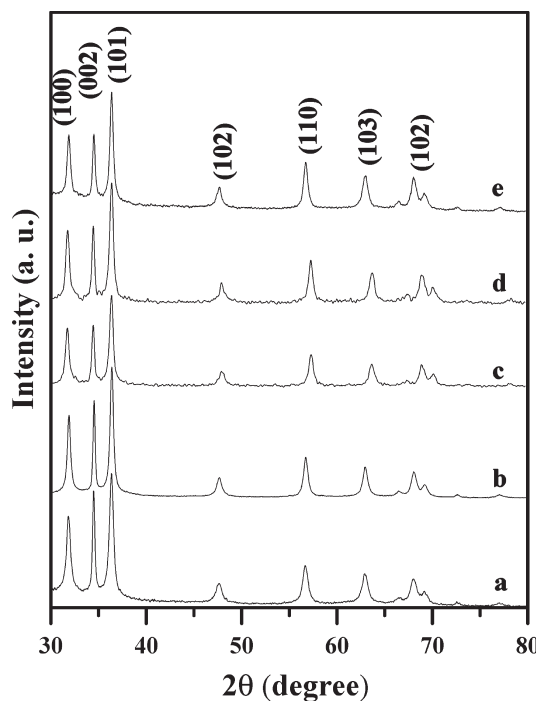


Figure 8. XRD patterns of different ZnO nanostructure samples from Table 3: (a) ZnO/As-11, (b) ZnO/As-1, (c) ZnO/As-12, (d) ZnO/As-13, and (e) ZnO/As-14.

presence of ascorbate the growth of ZnO nanostructures occurred preferentially along the (001) plane. The values of $R_{(002)/(101)}$ increase as the average diameter of the flowerlike ZnO nanostructures increases, which implies preferential growth along the (001) crystalline plane to give flowerlike morphology.

The energy-dispersive X-ray (EDX) spectrum was recorded from sample ZnO/As-1 as a representative case to determine the composition of the product. The quantitative EDX data obtained from several crystals revealed a Zn/O ratio of approximately 1.5:1 (Figure S2 in SI), within the error of EDX.⁶¹

FTIR Spectroscopy. To elucidate the growth mechanism for the formation of flowerlike ZnO nanostructures, it is very important to know the adsorbed species on its surface. Thus, FTIR characterization has been performed on ZnO nanostructures prepared with ascorbate (sample ZnO/As-1) (Figure 9c) or without ascorbate (sample ZnO-6) (Figure 9e). For comparison, we have also recorded the spectra of ZnAc₂ (Figure 9a) and neat sodium ascorbate (NaAs) (Figure 9b). The FTIR spectrum (Figure 9c) of flowerlike ZnO nanostructures (sample ZnO/As-1) exhibits a peak at 1715 cm⁻¹ corresponding to the >C=O stretching frequencies of the ascorbate ion. The position of the peak is slightly shifted from the >C=O stretching frequencies (~1704 cm⁻¹) of the neat ascorbate ion (Figure 9b).⁴¹ This result indicates the adsorption of ascorbate ion on the surface of ZnO. Another peak is observed at ~1627 cm⁻¹ that corresponds to a combination of the >C=C< stretching (~1598 cm⁻¹, Figure 9b) frequency of the neat ascorbate ion and the asymmetric >C=O stretching mode of the acetate ion at 1558 cm⁻¹, as shown in Figure 9a adsorbed on the surface of ZnO. The another peak at around 1397 cm⁻¹ for sample ZnO/As-1 (Figure 9c) can be assigned to the symmetric carboxylate stretching mode, which is shifted from that (1448 cm⁻¹) of the neat acetate ion as shown in Figure 9a. However, the spectra of samples ZnO-6 (prepared without ascorbate, Figure 9e)

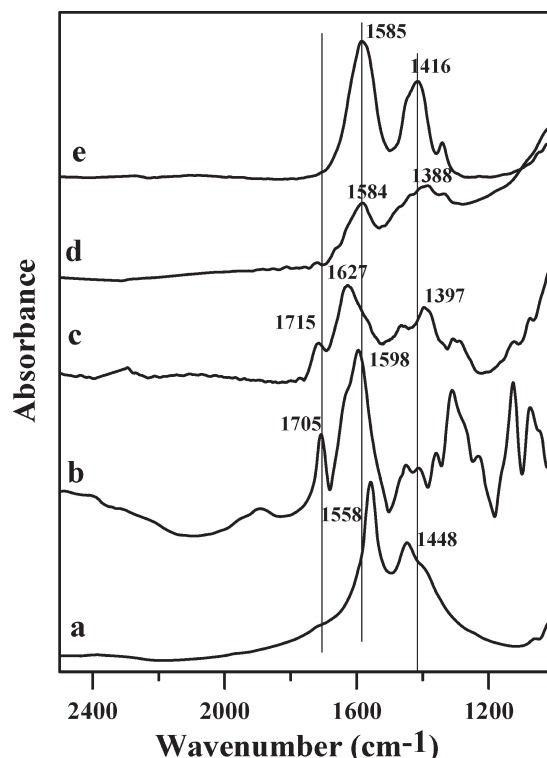


Figure 9. FTIR spectra of (a) neat ZnAc₂, (b) neat NaAs, (c) ZnO/As-1, (d) ZnO/As-1 after heating the sample for 12 h at 600 °C, and (e) ZnO-6.

and ignited ZnO/As-1 (ignited at 600 °C for 12 h, Figure 9d) exhibit peaks at ~1585 and ~1400 cm⁻¹ that correspond to asymmetric and symmetric carboxylate stretching frequencies of the adsorbed acetate ion (Figure 9a) on the ZnO surface and are also well matched with those reported elsewhere.⁶² Interestingly, these results indicate that after the ignition of sample ZnO/As-1 at 600 °C for 12 h the >C=O stretching frequency of the adsorbed ascorbate ion on the surface of ZnO vanishes (Figure 9d).⁶³ This result further proves that the ascorbate ions are adsorbed along with acetate ions on the ZnO surface. Earlier, Zhang et al. confirmed the adsorption of both oleylamine along with acetate ion on the surface of ZnO NPs, prepared by heating the mixture of oleylamine and ZnAc₂ using FTIR spectroscopy.⁶⁴

Possible Growth Mechanism. The above-mentioned FES-EM results of all of the ZnO samples, obtained after 30 min of reaction in the presence of ascorbate at 60 °C, clearly indicate the formation of only flowerlike ZnO nanostructures (otherwise, it is mentioned). However, one should not expect the formation of such morphology instantaneously, and there might be some intermediate morphology that ultimately transforms into the final structure. Thus, to elucidate the possible mechanism of the formation of such structures, the time-dependent morphological evolution of sample ZnO/As-1 was examined via FESEM. The reaction was first quenched by placing one drop of the reaction mixture on blotting paper to examine the morphology via FESEM with the expectation that we would be able to detect the intermediate morphology within 1 min of reaction. However, the FESEM image of sample ZnO/As-1 after 1 min of reaction clearly shows the formation of flowerlike morphology (Figure 10A). However,

(62) Vikulov, K.; Scarano, D.; Zecchina, A.; Coluccia, S. *J. Chem. Soc., Faraday Trans.* **1993**, *89*, 1127–1129.

(63) Labuayai, S.; Promarak, V.; Maensiri, S. *Appl. Phys. A: Mater. Sci. Process.* **2009**, *94*, 755–761.

(64) Zhang, Z.; Lu, M.; Xu, H.; Chin, W.-S. *Chem.—Eur. J.* **2007**, *13*, 632–638.

(61) Liu, X.; Afzaal, M.; Ramasamy, K.; O'Brien, P.; Akhtar, J. *J. Am. Chem. Soc.* **2009**, *131*, 15106–15107.

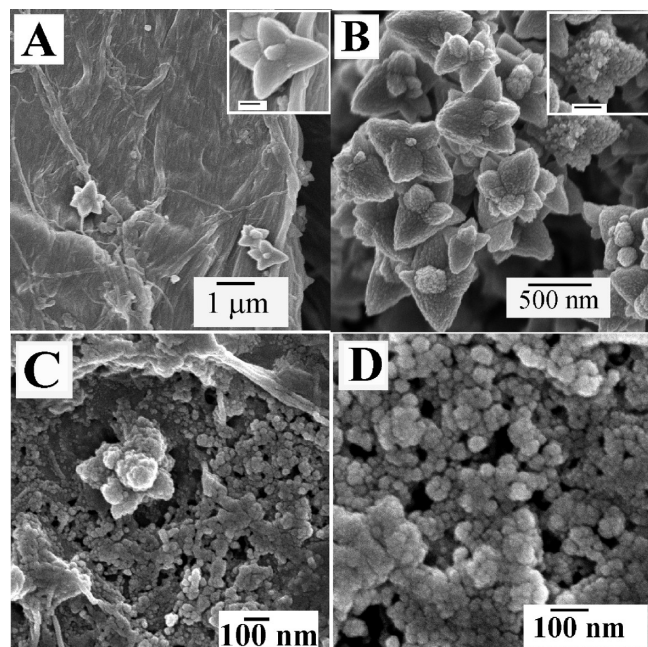


Figure 10. FESEM images of different hierarchical ZnO nanostructure samples prepared by varying the reaction time in the presence of ascorbate according to the conditions used for sample ZnO/As-1 in Table 1: (A) after 1 min and (B) after 2 min of reaction. (C, D) FESEM images (recorded after 10 min of reaction) of ZnO nanostructures prepared in the presence of ascorbate according to conditions used for sample ZnO/As-11 (Table 2) at 30 °C. (Insets) Enlarged views of the corresponding images; scale bars = 200 nm.

the population of the flower is much smaller. Furthermore, the sample obtained by quenching the same reaction after 2 min also shows a high population of flowerlike ZnO (Figure 10B). These results indicate that the rate of formation of flowerlike nanostructures is very fast at this temperature. Magnified FESEM images of a single flowerlike ZnO nanostructures obtained after 1 and 2 min of reaction, as given in the insets of Figure 10A,B respectively, clearly show that the petals of the flowers are not smooth. It seems that the petals are actually composed of assemblies of smaller spherical ZnO crystallites. The FESEM images of all other ZnO samples prepared with ascorbate, as shown in the insets of Figure 1, also show similar assembled morphology. Thus, we assume that the flowerlike ZnO nanostructures are formed through the assembly of spherical nanocrystallites, the formation mechanism of which will be discussed in detail later in this section. The FESEM images of the ZnO/As-11 sample (prepared at 30 °C) isolated after 10 min of reaction also show the presence of smaller spherical ZnO crystallites (Figure 10C,D). This result will be discussed further later in this section.

Furthermore, we have lowered the reactant concentration with the expectation that we would be able to monitor the intermediate morphology. The details of these reactions are provided in Table 4. In brief, different ZnO samples have been prepared by lowering the metal ion concentrations by 10, 20, and 100 times to that of sample ZnO/As-1 but maintaining fixed $[ZnAc_2]/[NaOH]/[\text{ascorbate}]$ ratios as in sample ZnO/As-1. These samples are designated as ZnO/As-15, ZnO/As-16, and ZnO/As-17, respectively (Table 4). Interestingly, FESEM images of samples ZnO/As-15 and ZnO/As-16 show only spindle-shaped nanostructures (Figure 11A,B). It should be noted that no flowerlike ZnO nanostructures were observed in these cases. The sizes [maximum end-to-end distance (length)] of the spindles are in the

ranges of 500–700 and 700–900 nm for samples ZnO/As-15 and ZnO/As-16, respectively. It seems that these spindles are the intermediates on the pathway of formation of flowerlike ZnO nanostructures.^{52,65} It was noted that under these reactant conditions no other morphologies were observed, no matter what the reaction time. When the metal ion concentration was further lowered by 100-fold (sample ZnO/As-17 in Table 4), interestingly, we have observed the formation of mostly smaller spherical/quasi-spherical ZnO nanocrystallites along with a few spindles, as can be seen in the FESEM provided in Figure 11C. The diameters of these spherical nanocrystallites are in the range of 20–30 nm. However, the surfaces of the spindles are not very smooth and are seemingly composed of spherical nanocrystallites, as could be clearly seen from the high-magnification image shown in Figure 11D. The dimensions of these nanocrystals are similar to that of free spherical nanocrystallites observed on the same image (inset of Figure 11D).

Furthermore, to determine whether the formed spherical and spindle-shaped ZnO nanostructures at lower precursor concentrations are the probable intermediates on the pathway to large flowerlike nanostructures, we have carried out two additional reactions. For this, we have taken the as-prepared suspension of ZnO nanostructures (sample ZnO/As-16) after 30 min of reaction as the seed solution. We have then added fresh ZnAc₂, NaOH, and ascorbate solution separately to these solutions according to the recipes provided for samples ZnO/As-16-m1 and ZnO/As-16-m2, respectively (Table 4), and the mixture was held at 60 °C for an additional 30 min. The purified and dried ZnO samples were then analyzed through FESEM. The FESEM image of sample ZnO/As-16-m1 (Figure 11E) shows the growth of spherical nanocrystallites from the middle part of the spindle-shaped nanostructures along with some fully grown flowerlike nanostructures (cf. Figure 11E,B). When the concentration of the added reactant is high (sample ZnO/As-16-m2), we have observed the formation of only flowerlike ZnO nanostructures (Figure 11F). These results clearly indicate that the flowerlike ZnO nanostructures are formed from the spindle-shape ZnO intermediates.

It is known that the reaction rate usually increases with increasing temperature. In the present study, we have observed that the rate of formation of flowerlike ZnO nanostructures was so high at 60 °C that we would not be able to detect the intermediate products. Hence, we repeated the preparation of ZnO nanostructures at lower temperature (30 °C) with the expectation that the rate of formation of flowerlike ZnO nanostructures would be lower at lower temperature and thus it would also be possible to monitor the morphology of ZnO formed in the early stages of the reaction. As mentioned above, sample ZnO/As-11, obtained after 30 min of reaction at 30 °C, showed only flowerlike morphology (Figure 3A). However, the FESEM image of the same sample isolated after 10 min of reaction at the same temperature (30 °C) shows predominantly spherical/quasi-spherical ZnO nanocrystallites with diameter ranging from 20 to 30 nm along with some flowerlike nanostructures (Figure 10C,D). The flowerlike nanostructures are formed through some kind of assembly of these smaller nanocrystallites. Note that these types of free spherical nanocrystallites are absent in the sample obtained after 30 min of reaction (Figure 3A). However, we were unable to detect the formation of the spindle as an intermediate product at this temperature. This might be due to the fact that after the formation of spherical nanocrystallites the rate of assembly into flowerlike nanostructures is so fast that we are unable to detect such a spindle intermediate.

For a better understanding of the growth mechanism of our ZnO nanostructures, we have examined the obtained differently

(65) Peng, Z. A.; Peng, X. *J. Am. Chem. Soc.* **2001**, *123*, 1389–1395.

Table 4. Reaction Recipe for ZnO Nanostructures Prepared at Lower Concentrations of Reactants and Their and Characterization Data^a

sample name	[ZnAc ₂] (M)	[NaOH] (M)	[ascorbate] (M)	shape	size (nm) ^c	pH
ZnO/As-15	0.001	0.005	0.0001	spindle	500–700 ^d	10.5
ZnO/As-16	0.0005	0.0025	0.00005	spindle	700–900 ^d	9.5
ZnO/As-17	0.0001	0.0005	0.00001	mixture of small spheres and spindle		7.5
^b ZnO/As-16-m1	0.002	0.01	0.0002	spindle with debris		11.0
^b ZnO/As-16-m2	0.004	0.02	0.0004	flower and spindle with debris		11.5

^a Temperature = 60 °C. Time = 30 min. ^b The as-prepared suspension of sample ZnO/As-16 was taken after 30 min of reaction, and the additional precursors were added separately according to samples ZnO/As-16-m1 and ZnO/As-16-m2 and then heated for 30 min at the same temperature. ^c Sizes were determined from FESEM pictures (particle count = 25). ^d Maximum end-to-end distance (length) of the spindlelike ZnO.

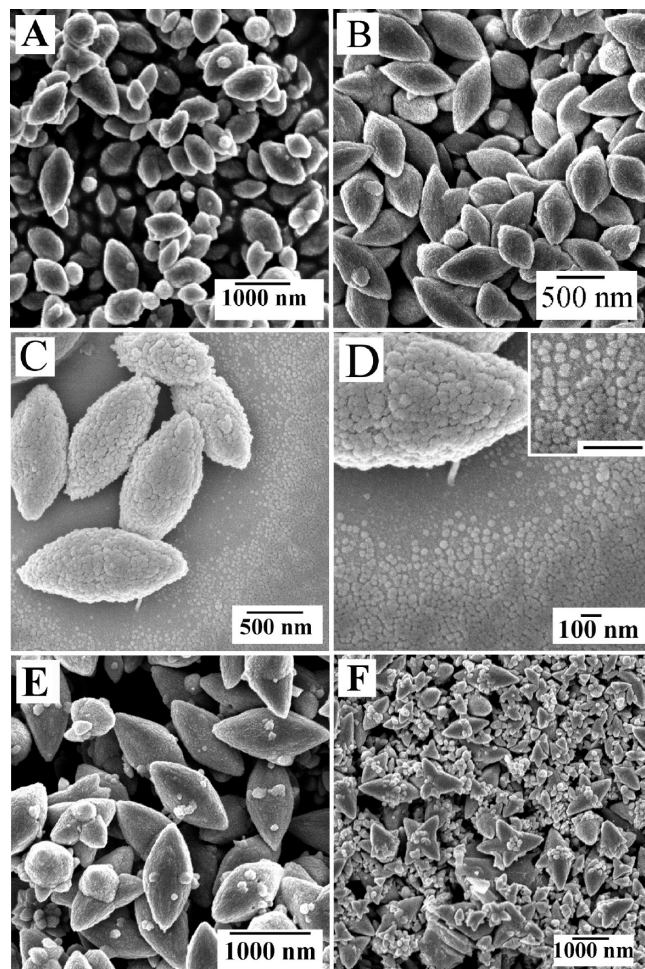


Figure 11. FESEM images of different hierarchical ZnO nanostructure samples prepared at lower metal ion concentrations (Table 4): (A) ZnO/As-15, (B) ZnO/As-16, (C, D) ZnO/As-17, (E) ZnO/As-16-m1, and (F) ZnO/As-16-m2. The inset of panel D shows enlarged views of the corresponding images; scale bar = 200 nm.

shaped ZnO nanostructures via TEM. Figure 12A shows the TEM image of representative flowerlike ZnO nanostructures (sample ZnO/As-1), which clearly revealed that the shape of the ZnO nanostructures resembles starlike morphology. This is due to the fact that TEM images basically provide a 2D projection of a 3D object, and hence the flowerlike morphology as observed through FESEM appears to be a star. The magnified TEM image of a single particle (inset of Figure 12A) indicates that the edges of these nanostructures are not smooth and are composed of assemblies of smaller nanocrystallites, as also observed earlier in the FESEM images.

Figure 12B shows the selected-area electron diffraction (SAED) pattern recorded from a specified portion (red marked area) of a single flowerlike ZnO given in the inset of Figure 12A,

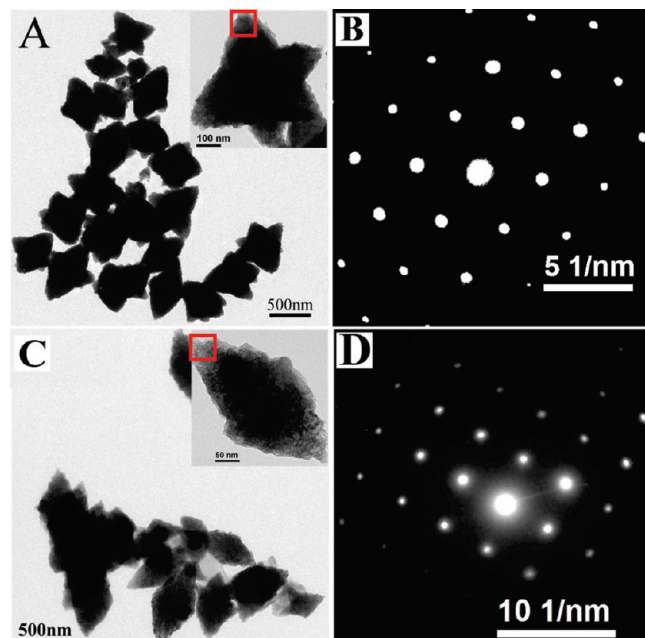


Figure 12. (A) TEM image of flowerlike ZnO nanostructures (sample ZnO/As-1). (B) SAED pattern of flowerlike ZnO nanostructures (sample ZnO/As-1) taken from the specified portion (red box) in the inset of panel A. (C) TEM image of spindle-shaped ZnO nanostructures (sample ZnO/As-15). (D) SAED pattern of spindle-shaped ZnO nanostructures (sample ZnO/As-15) taken from the specified portion (red box) in the inset of panel C. Insets in panels A and C represent the magnified images of the respective samples.

which indicated that the formed ZnO nanostructures are very crystalline and consist of hexagonal phases. Additionally, we have also taken SAED patterns from some other portions of the flowerlike ZnO nanostructures, and these patterns are similar to that in Figure 12B as given in Figure S3 in SI. Figure 12C shows the TEM image of spindle-shaped ZnO nanostructures (sample ZnO/As-15 in Table 4). Unfortunately, the 3D spindlelike ZnO, as observed via FESEM, had rectangular morphology under TEM (cf. Figures 11A and 12C). Again, the surfaces of such spindles are not smooth and look similar to those of the petals of flowers, as can also be seen in the TEM image of sample ZnO/As-1 (inset of Figure 12A). The SAED pattern (Figure 12D) taken from the specified portion (red box) of the spindle-shaped ZnO nanostructures depicted in the inset of Figure 12C indicates that these spindle-shaped ZnO nanostructures are very crystalline and consists of hexagonal phases. Additional SAED patterns acquired from different portions of a spindle-shaped ZnO nanostructure are provided in Figure S4 in SI. These patterns are very similar to that presented in Figure 12D. It should be noted that these flowerlike nanostrucutes are formed through preferential growth along the (001) plane, as indicated by the XRD results

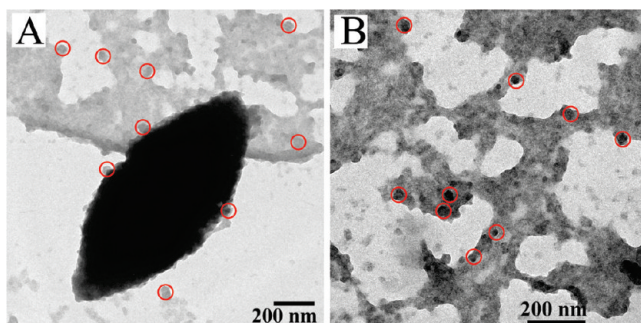
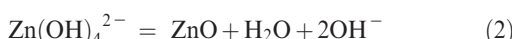


Figure 13. (A, B) TEM images of the ZnO/As-17 sample (Table 4) taken from different portions of the grid.

mentioned above. This was further confirmed from the analysis of HRTEM images of certain portions of spindlelike and flowerlike nanostructures, which show the presence of clear lattice fringes with an interplanar spacing of 0.26 nm corresponding to the (001) plane of ZnO nanostructures (Figure S5 in SI).

Figure 13 shows the TEM images of sample ZnO/As-17 taken from different portions on a grid that again show the presence of spindle-shaped ZnO along with some spherical particles (as shown by red circles) with diameter ranging from 20 to 30 nm. In this case, the surfaces of the spindle-shaped ZnO nanostructure are also not smooth. It seems that such spindle-shaped nanostructures might form by the assembly of the small spherical particles (shown by circles) present in this system (Figure 13). These results are consistent with the results obtained from FESEM studies.

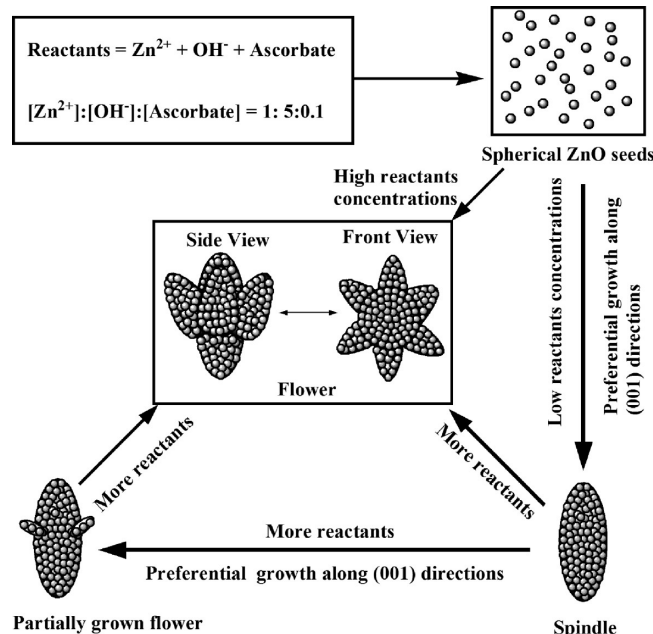
On the basis of the information that we have gathered via FESEM, XRD, and TEM studies, we can propose a probable mechanism for the formation of flowerlike ZnO nanostructures, which is pictorially represented in Scheme 1. According to literature reports, the growth unit for the formation of ZnO nanostructures by the alkaline hydrolysis of Zn^{2+} is the $[Zn(OH)_4]^{2-}$ ion,⁶⁶ which further undergoes dehydration according to the following equations to produce ZnO.



In a very early stage, as this dehydration reaction progresses, more and more ZnO clusters are formed in the solution. When the supersaturation state is attained in the reaction medium, nucleation starts (Scheme 1) and the thermodynamically stable (lower surface energy) spherical/quasi-spherical ZnO seeds ($\sim 20\text{--}30\text{ nm}$) start to form in the solution as mentioned elsewhere.^{60,67} We are able to identify these spherical ZnO seeds by lowering the reactant concentrations (Figure 11C,D). We are also able to identify spherical particles for sample ZnO/As-11 (prepared at 30 °C) isolated after 10 min of reaction (Figure 10C,D).

As soon as the primary nanocrystallites (seeds) are formed, they rapidly assemble to give larger, more-stable secondary aggregates. In our case, these secondary aggregates of ZnO may take the shape of spindles or flowers (Figures 10 and 11). This type of aggregation of smaller crystallites to form larger nanostruc-

Scheme 1. Schematic Representation of the Probable Growth Mechanism of Flowerlike ZnO Nanostructures



tures has also been suggested by earlier researchers to explain the anisotropic growth of metal oxides and metal sulfides.^{16,68} It is well known that for kinetically controlled products the flux of reactants largely determined the shape of the particles formed.⁶⁰ With the increase in the flux of reactant concentration, a gradual evolution of shape occurs through zero dimensions to one dimension and so on to three dimensions as reported by Peng et al.⁶⁵ In our case, the initially formed spherical/quasi-spherical ZnO nanocrystallites are assembled through oriented attachment in a particular plane during growth, as confirmed by the high-resolution TEM results of a certain portion of both spindle and flower-shaped nanostructures that show only the (001) plane.⁶⁹ The flowerlike nanostructures are formed when further aggregation starts, which is promoted by an even higher flux of ZnO monomers (ions, atoms, or molecules). In this step, the spherical/quasi-spherical nanocrystallites were assembled specifically on the middle of the spindle-shaped ZnO, as could be seen from the FESEM picture (Figure 11E) shown earlier.

It is known that in the nucleation stage the growth of the ZnO nanostructures largely depends on the concentration of the reactants irrespective of the presence of any foreign agent such as surfactant, polymer, or other additives in the medium. However, at the time of secondary particle formation, the additives are adsorbed onto preferred planes and alter the growth kinetics. Generally, ZnO possess three basal planes such as a polar (001) plane and two nonpolar (110) and (100) planes,⁶⁶ among which the polar (001) plane is most reactive until any complexing/passivating agent compensates for its surface energy.^{57,70} Therefore, in our case, in the nucleation stage, growth along all preferred directions might occur to produce spherical/quasi-spherical seeds with diameters of 20–30 nm. However, it is expected that the ascorbate ion might adsorbs onto the side of the (001) plane, lowering the activation energy needed for nucleation and crystal growth and directing preferential growth along the (001) plane. This preferential growth probably occurs through oriented attachment along the (001) plane, as also

(66) Li, W.-J.; Shi, E.-W.; Zhong, W.-Z.; Yin, Z.-W. *J. Cryst. Growth* **1999**, *203*, 186–196.

(67) Lee, S.-M.; Cho, S.-N.; Cheon, J. *Adv. Mater.* **2003**, *15*, 441–444.

(68) Park, J.; Privman, V.; Matijevic, E. *J. Phys. Chem. B* **2001**, *105*, 11630–11635.

(69) Alivisatos, A. P. *Science* **2000**, *289*, 736–737.

(70) Cao, B.; Cai, W. *J. Phys. Chem. C* **2008**, *112*, 680–685.

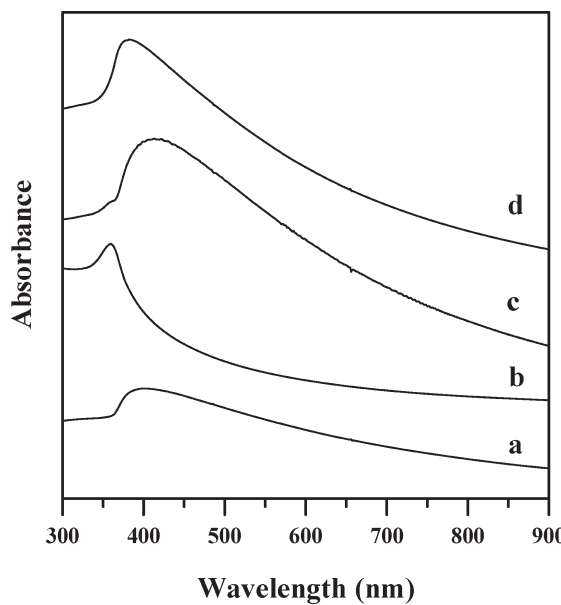


Figure 14. UV-vis absorption spectra of an aqueous suspension of different ZnO samples with different shapes: (a) ZnO/As-17 (spherical), (b) ZnO/As-16 (spindle), (c) ZnO/As-1 (flower), and (d) ZnO-6 (undefined morphology).

confirmed via high-resolution TEM (mentioned above) (i.e., in the z direction to produce spindle-shape nanostructures). The adsorption of the ascorbate ion on the surface of ZnO has been confirmed by FTIR spectroscopy as discussed above (Figure 9). After the formation of spindles, the spherical nanocrystallites assembled through oriented attachment again along the (001) plane of the spindles to form flowerlike ZnO nanostructures, as indicated by XRD and high-resolution TEM results (Figure S5 in SI). This mechanism also nicely explains why larger flowerlike nanostructures are formed at higher ascorbate concentration. Actually, at higher ascorbate concentration, the (001) growth front of ZnO is active for a longer time, giving rise to larger ZnO flowers. Several researchers have also demonstrated the formation of this type of larger nanostructure by the assembly of smaller nanocrystallites through oriented attachment.^{16,71} However, at this point, we do not have any answer to why the nanocrystallites are assembled only through the middle of the spindle to produce flowerlike structures, as observed in the ZnO/As-16-m1 sample (Figure 11E).

UV-Vis Absorption and Photoluminescence Spectroscopy. The optical properties of the redispersed aqueous suspensions of ZnO nanostructures prepared with or without ascorbate were studied via UV-vis absorption and photoluminescence (PL) spectroscopy. Figure 14 shows the UV-vis spectra of as-prepared ZnO samples with varying morphology: ZnO/As-17 (spherical), ZnO/As-16 (spindle), and ZnO/As-1 (flower). For comparison, the spectrum of the ZnO sample (ZnO-6, undefined morphology) prepared without ascorbate was also acquired and was appended as Figure 14d. All of the spectra are dominated by an absorption band in the lower-wavelength region, followed by long tailing due to scattering.⁶⁴ For example, the ZnO/As-17 sample (spherical) shows a broad absorbance band with its maximum at around 395 nm (Figure 14a). The ZnO spindle (ZnO/As-16) shows a sharp absorption at $\lambda_{\text{max}} = 360$ nm (Figure 14b). However, the spectrum of flowerlike ZnO (sample ZnO/As-1) exhibits a broad band

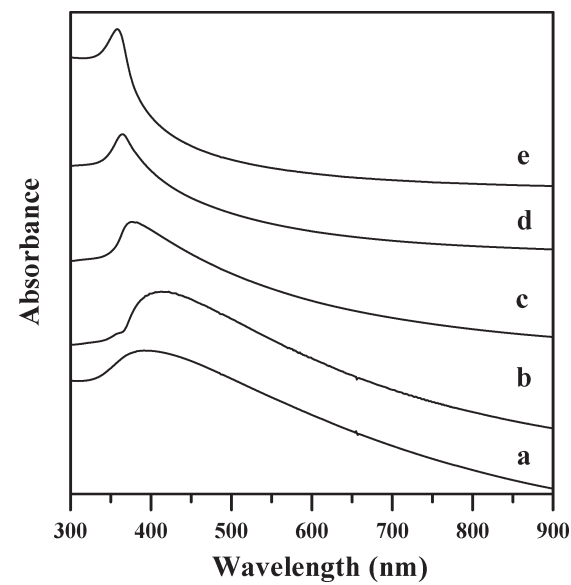


Figure 15. UV-vis absorption spectra of aqueous suspensions of different ZnO samples prepared at different temperatures: (a) ZnO/As-11 at 30 °C, (b) ZnO/As-1 at 60 °C, (c) ZnO/As-12 at 70 °C, (d) ZnO/As-13 at 80 °C, and (e) ZnO/As-14 at 90 °C.

with $\lambda_{\text{max}} = 405$ nm (Figure 14c). The spectrum of sample ZnO-6 with undefined morphology also shows an absorption band with $\lambda_{\text{max}} = 379$ nm, followed by long tailing due to scattering (Figure 14d). Kumari et al. have also observed this type of broad absorption band for their hierarchical ZnO nanostructures.⁷²

Figure 15 shows the absorption spectra of samples ZnO/As-11, ZnO/As-1, ZnO/As-12, ZnO/As-13, and ZnO/As-14 prepared at different temperatures. The flowerlike ZnO nanostructures prepared at 30 and 60 °C (samples ZnO/As-11 and ZnO/As-1, respectively) exhibit broad absorption bands at around 390 and 405 nm, respectively, followed by a long tail (Figure 15a,b). However, the spectra of ZnO samples prepared at 70 °C (sample ZnO/As-12), 80 °C (sample ZnO/As-13), and 90 °C (ZnO/As-14) with undeveloped flower-shaped, spindle-shaped, and spherically shaped morphology exhibit sharp bands at 377 nm (Figure 15c), 364 nm (Figure 15d), and 358 nm (Figure 15e), respectively. It was interesting that the absorption peaks became sharper and blue-shifted from 405 to 358 nm as the sample-preparation temperature was increased from 60 to 90 °C (Figure 15). This is understandable because the sizes of the particles decrease with increasing reaction temperature and consequently the band gap between the valence band and the conduction band also increases.⁷³ Consequently, a blue shifting of the absorption peak in the UV-vis spectra of these samples was observed.

The room-temperature PL spectra of the ZnO samples in a water suspension were acquired by excitation at 340 nm and are presented in Figure 16. The PL spectra of the flowerlike ZnO nanostructures prepared in the presence of ascorbate (samples ZnO/As-1 and ZnO/As-2) were dominated by a sharp emission band having a λ_{max} at 372 nm along with a broad, weak band in the higher-wavelength region of 500–660 nm (Figure 16A). The emission band in the lower-wavelength region is assigned as the near-band-edge (NBE) emission band, which corresponds to the radiative annihilation of excitons as reported elsewhere.^{1,19} The weak, broad emission band in the higher-wavelength region

(71) Li, L.-S.; Walda, J.; Manna, L.; Alivisatos, A. P. *Nano Lett.* **2002**, *2*, 557–560.

(72) Kumari, L.; Li, W. Z. *Cryst. Res. Technol.* **2010**, *45*, 311–315.

(73) Cozzoli, P. D.; Curri, M. L.; Agostiano, A.; Leo, G.; Lomascolo, M. *J. Phys. Chem. B* **2003**, *107*, 4756–4762.

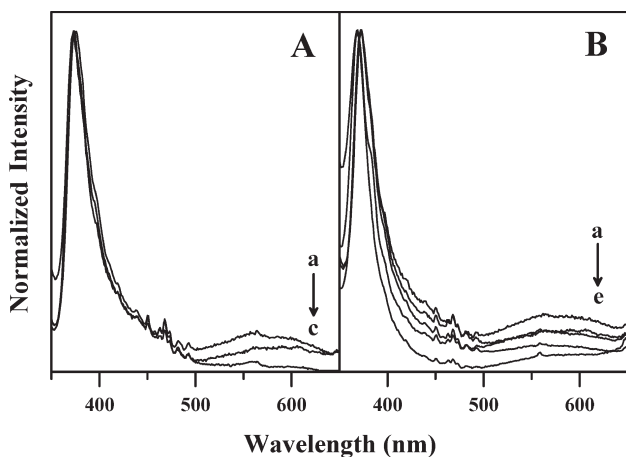


Figure 16. Photoluminescence spectra of different ZnO nanostructures acquired from a redispersed aqueous suspension. (A) Samples prepared with varying ascorbate concentration: (a) ZnO/As-2, (b) ZnO/As-1, and (c) ZnO-6. (B) Samples prepared at different temperatures: (a) ZnO/As-11, (b) ZnO/As-1, (c) ZnO/As-12, (d) ZnO/As-13, and (e) ZnO/As-14.

is termed a deep-level or trap-state emission band, which might be the superposition of green emission around 520 nm and a near-yellow emission around 640 nm as reported elsewhere.^{35,74} This trap-state emission is usually associated with various types of defects resulting from various oxygen vacancies in the valence band of ZnO nanostructures.^{50,74} The relative intensity of this broad emission band in the higher-wavelength region with respect to that in the lower-wavelength region increases with the increase in ascorbate concentration in the medium (cf. Figure 16Aa,Ab). However, the PL spectrum of sample ZnO-6 (prepared without ascorbate), having no flowerlike morphology, exhibits only the NBE emission band (Figure 16Ac). These results indicate that the structural defects in sample ZnO-6 are almost negligible and the proportion of defect states in the formed ZnO nanostructures (samples ZnO/As-1 and ZnO/As-2) increases as the concentration of ascorbate ion in the medium increases. This might be due to the fact that as the concentration of ascorbate is increased the number of defect states during crystal formation is also increased. These defect states might originate from the adsorption of ascorbate ion on the crystal planes of the growing ZnO nanostructures, as confirmed by the FTIR spectroscopy discussed above (Figure 9). As the concentration of ascorbate in the reaction medium increased, the chance of its adsorption on the ZnO surface increased, which might result in an increase of defects due to oxygen vacancies.

The PL spectra of samples ZnO/As-11, ZnO/As-1, ZnO/As-12, ZnO/As-13, and ZnO/As-14 prepared at different reaction temperatures such as 30, 60, 70, 80, and 90 °C, respectively, are presented in Figure 16B. The PL spectra of samples ZnO/As-11 (Figure 16Ba), ZnO/As-1 (Figure 16Bb), and ZnO/As-12 (Figure 16Bc) prepared at 30, 60, and 70 °C, respectively, with flowerlike morphology exhibited NBE bands at the same position (372 nm). However, a slight blue shift of this emission peak was observed for samples ZnO/As-13 (369 nm) (Figure 16Bd) and ZnO/As-14 (368 nm) (Figure 16Be) prepared at 80 and 90 °C, respectively, having spindle and spherical morphology. The fwhm of the sharp band (368 nm) for the ZnO/As-14 sample was measured to be 15 nm. The normalized intensity (with respect to the emission corresponding to the NBE band) of the trap-state

Scheme 2. Friedel–Crafts Acylation of Anthracene with Benzoyl Chloride Using ZnO as a Catalyst

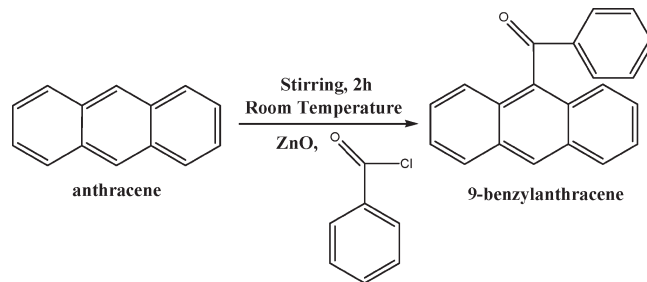


Table 5. Study of the Catalytic Activity of Different Hierarchical ZnO Nanostructures in the Acylation Reaction of Anthracene with Benzoyl Chloride

sample name	shape	catalyst (mmol)	anthracene (mmol)	benzoyl chloride (mmol)	time (min)	yield (%)
ZnO/As-1	flower	0.1	1	2	120	50
ZnO/As-1	flower	0.5	1	2	120	65
ZnO/As-14	spherical	0.1	1	2	120	40
ZnO/As-14	spherical	0.5	1	2	120	60

emission band (~500–660 nm) systematically decreased when the sample-preparation temperature was increased, which is in accordance with the results reported elsewhere by other researchers.⁷⁴ These results show that the defect states in the synthesized ZnO samples decrease as the reaction temperature increases.

Catalytic Activity of ZnO Nanostructures in the Friedel–Crafts Acylation of Anthracene. As we have mentioned in the Introduction, one of the most important applications of nanostructured ZnO is its use as a photocatalyst to remove organic and biological hazards dissolved in water.^{3,39} However, the catalytic activity of such ZnO nanostructures toward organic reactions has been less frequently studied. Thus, to determine whether the obtained ZnO nanostructures in the present study are catalytically active, we have performed the Friedel–Crafts acylation reaction of anthracene with benzoyl chloride as a model reaction using the flowerlike ZnO nanostructure (sample ZnO/As-1) (Scheme 2). The yield was measured from the analysis of the ¹H NMR spectra of the reactants and the products. Generally, neat anthracene shows one peak at around δ = 8.42 corresponding to the H atoms at the C-9 and C-10 positions of pure anthracene (Figure S6 in SI). However, this peak shifts downfield at δ = 8.57 (Figure S7 in SI) when the acylation of anthracene with benzoyl chloride takes place at the C-9 position. The intensity ratio between these two peaks will give the amount of the product (9-benzylanthracene) formed. The yield of the product was measured from the analysis of NMR spectra of the crude product as shown in Figure S8 in SI. A detailed calculation of the yield measurement is given in the Supporting Information. The yield of the acylated product (9-benzylanthracene) was 65% when 0.5 mmol of flowerlike ZnO nanostructures was used. For comparison, we have also performed the same reaction using spherical ZnO nanostructures (sample ZnO/As-14) prepared at 90 °C. In this case, the yield of the product (9-benzylanthracene) was about 60% (Table 5) when the same amount of catalyst (0.5 mmol of sample ZnO/As-14) was used. When the same catalytic conversion was carried out using 0.1 mmol of ZnO samples, the yields of 9-benzylanthracene were calculated to be 50 and 40% for flowerlike (sample ZnO/As-1) and spherical nanostructures (sample ZnO/As-14), respectively. A comparison

(74) Studenikin, S. A.; Golego, N.; Cocivera, M. *J. Appl. Phys.* **1998**, *84*, 2287–2294.

of the results provided in Table 5 indicated that the catalytic properties of flowerlike ZnO nanostructures were slightly better than their spherical counterpart. This difference in catalytic activity might arise from the hyperbranched nature of the flowerlike ZnO nanostructures. It has also been reported that the materials (e.g., gold, iron oxide, etc.) with flowerlike nanostructures are catalytically more active than their spherical counterpart because of their higher surface area.^{53–56} Another possible reason for the higher catalytic activity may be due to the larger number of defect states present in the flowerlike ZnO than in spherical ZnO, as evident from the PL studies of these two differently shaped nanostructures mentioned above (Figure 16B). Du et al. have also reasoned that the higher catalytic activities of ZnO nanostructures are probably due to the presence of larger numbers of defect states in the nanostructures.¹⁸

Furthermore, it has been reported that the shape of nanosstructured Pt changes after catalysis.⁷⁵ Thus, to ascertain the fate of our ZnO catalyst after the reaction, we have recovered the catalyst from the reaction mixture and the dried isolated mass has been analyzed by XRD and FESEM. The FESEM images revealed that the initial morphology of both flowerlike and spherical ZnO nanostructures was destroyed during/after catalysis (Figure S9 in SI). The XRD patterns of the isolated mass from both ZnO flowers and spheres after catalysis were similar and were associated with some additional peaks along with the characteristic peaks of ZnO (Figure S10 in SI). These additional peaks correspond to impurities such as Zn(OH)₂ and Zn(OH)Cl, as determined by JCPDS files (file nos. 38-0356 and 32-1467, respectively). Thus, we believe that this reaction takes place in two stages. In the first stage, flowerlike/spherical ZnO nanostructures catalyzed the acylation reaction of anthracene with benzoyl chloride and produced 9-benzylanthracene and HCl gas. In the second stage, the produced HCl eventually reacts with ZnO nanostructures and destroys their morphology. Therefore, we may conclude that the slightly higher catalytic activity of flowerlike ZnO compared to that of their spherical counterpart is due to a higher surface-to-volume ratio and/or the presence of a larger number of defect states. Because the impurities are formed in the second stage of reaction, we can certainly conclude that the slightly higher activity of the flower is not due to the presence of such formed impurities. Detailed studies of the catalytic activities of differently shaped ZnO nanostructures in different organic reactions and their stability after catalysis are currently underway.

Conclusions

We report a simple solution-phase method of preparing mainly flowerlike ZnO nanostructures with controllable sizes using ascorbate as a shape-directing/capping agent at 30 and 60 °C. We have varied the concentrations of zinc precursors, alkali, and

ascorbate as well as the reaction temperature to study their effects on the size/shape of the formed ZnO nanostructures. We have observed that different shapes of hierarchical ZnO nanostructures such as flowerlike, spindlelike, and spherical can be obtained with an increase in synthesis temperature from 60 to 90 °C. We have also studied the effects of other organic salts as capping agents on the shape of hierarchical ZnO nanostructures. The adsorption of the ascorbate ion and its role in the preferential growth of ZnO crystals was studied using FTIR spectroscopy and TEM. XRD studies confirmed the crystalline nature and purity of the formed ZnO nanostructures. Controlled experiments without ascorbate confirmed that ascorbate ions regulate the growth of flowerlike ZnO nanostructures. We are also able to identify intermediate morphologies such as spherical/quasi-spherical and spindle-shaped nanostructures, which were very much on the pathway of formation of flowerlike ZnO nanostructures by changing the concentration of precursors and the shape-directing agent. On the basis of these results, we have provided a possible growth mechanism for flowerlike ZnO nanostructures. The PL results show that the density of defect states in the formed ZnO increases with the increase in ascorbate concentration and decreases with the increase in reaction temperature. The as-synthesized differently shaped ZnO nanostructures have been successfully used as catalysts in the Friedel–Crafts acylation of anthracene with benzoyl chloride. The yield of the product was measured through NMR spectroscopy, and the results show that flowerlike ZnO nanostructures are catalytically slightly more active than spherical nanostructures.

Acknowledgment. M.R., Md.H.R., T.K.P., and E.D. thank CSIR, Government of India, for providing fellowships. We also thank the reviewer who offered constructive criticism and suggested additional experiments, which were duly performed as described in the text. This research was supported by grants from CSIR, New Delhi, India. Thanks are also due to the financial support from the DST, New Delhi, India, under the Nanoscience and Nanotechnology Initiative.

Supporting Information Available: ¹H NMR data of sodium ascorbate, sodium tartarate, and sodium tyrosinate. FESEM images of ZnO nanostructures prepared under different reaction conditions. EDX spectra of ZnO nanostructures. SAED patterns from different portions of flowerlike and spindle-shaped ZnO nanostructures. High-resolution TEM images of both the flowerlike and spindle-shaped nanostructures. ¹H NMR spectra of pure anthracene, purified 9-benzylanthracene, and the crude product containing both anthracene and 9-benzylanthracene. Calculation of the yield measurement from NMR spectra. FESEM pictures and XRD pattern of ZnO after the catalysis reaction. This material is available free of charge via the Internet at <http://pubs.acs.org>.

(75) Narayanan, R.; El-Sayed, M. *J. Phys. Chem. B* **2005**, *109*, 12663–12676.